TRANSMISSION LINE MODEL OF THE DISTRIBUTED HETEROJUNCTION BIPOLAR TRANSISTOR

L. L. Liou
Avionics Directorate
Wright Laboratory
Wright-Patterson Air Force Base, OH 45433-7322

ABSTRACT

The distributed nature of heterojunction bipolar transistor was modeled using the transmission line method. Admittances due to the bipolar junction, base metal schottky contact, base and emitter contact resistances, were taken into account. Coupled differential equations describing the distributed nature of the junction potentials were derived. A numerical scheme was developed to solve the equations, and microwave parameters were calculated. The model can be applied to design HBT layouts for high microwave performance.

INTRODUCTION

Heterojunction bipolar transistors (HBTs) are widely used as the active devices in microwave integrated circuits. The layout design of this active device is important in order to realize its potentially high performance in microwave frequencies. The emitter layout design includes multiple-emitter-fingers and a circular emitter dot array[1]. In each design, the emitter mesa is in the shape of either a rectangular finger or a circular dot, and is enclosed by the self-aligned base metal. For microwave power applications, the important considerations in the emitter design are thermal and distributed effects. These two effects lead to different design rules, and trade-offs are usually required in designing the emitter geometry. For the same active emitter area, the emitter-finger design, because of its heat source compactness, has a larger thermal resistance compared to the emitter-dot-array design. However, the latter design usually contains a larger base-emitter capacitance, due to the larger extended length of the emitter-dot-array. While thermal effects of HBTs have been intensively studied[2,3,4], there has been only limited study on the distributed nature of HBTs[5].

In this study, we establish a transmission line model (TLM) to study the distributed nature of the emitter, base and collector potentials, and their effects on the microwave parameters of the HBT.

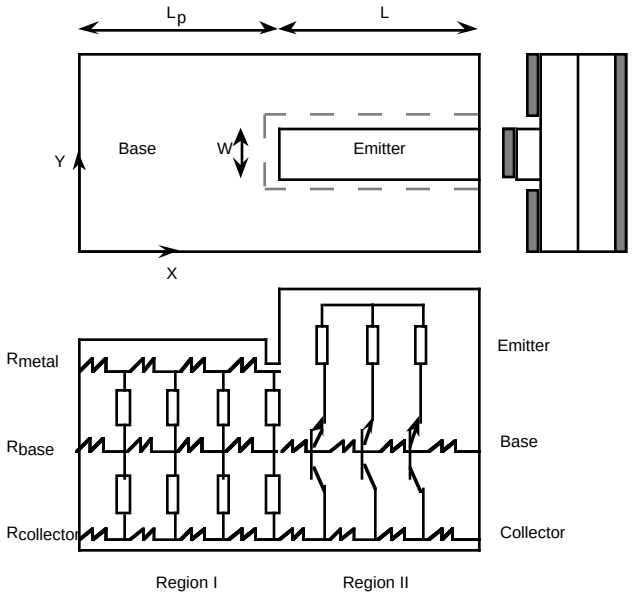

Fig. 1: The schematic diagram of the top view and the cross-section of the distributed HBT. The small boxes and resistors represent the infinitesimal impedance elements.

THEORY

Besides the distributed nature of the potentials, the theory also takes into account the base, and emitter contact (ballast) resistance, and capacitance of the schottky junction at the base metal and semiconductor interface. In Fig. 1, we show the top-view and the cross-section of a one-emitter-finger HBT. The domain is divided into two regions. Region I contains the base contact and the gap regions, and Region II is the emitter mesa region. Each region has three layers of horizontal networks. In Region I, these networks represent base metal, intrinsic base and sub-collector layers. They are vertically interconnected by infinitesimal passive elements of a resistor in parallel with a capacitor. In Region II, these networks represent emitter, intrinsic base and sub-collector layers, and they are vertically interconnected by infinitesimal bipolar junction elements.

The TLM technique is applied on each network in both regions. Three coupled partial differential

0-7803-4603-6/97/$5.00 (c) IEEE

equations are derived for the intrinsic base potential, v_i, base metal potential, v_b, and the collector potential v_c. They are given by:

$$\nabla^2 v_i = r_{sh}(a_{ii}v_i + a_{ib}v_b + a_{ic}v_c) \text{ in Region I}$$
$$\nabla^2 v_i = r_{sh}(b_{ii}v_i + b_{ic}v_c + b_{ie}v_e) \text{ in Region II}$$
$$\nabla^2 v_b = r_m y_{bi}(v_b - v_i) \text{ in Region I}$$
$$\nabla^2 v_c = r_{col} y_{ci}(v_c - v_i) \text{ in Region I}$$
$$\nabla^2 v_c = r_{col}(c_{cc}v_c + c_{ci}v_i + c_{ce}v_e) \text{ in Region II}$$

where ∇^2 is the two-dimensional Laplacian operator, r_{sh}, r_m and r_{col} are the base, base metal, and sub-collector sheet resistance, respectively, and v_e is the distributed emitter potential. For common-emitter mode operation, we assume v_e to be zero. The coefficients in the above equations are derived and they are given in the following:

$$a_{ii} = G_{bi} + G_{ci}$$
$$a_{ib} = -G_{bi} \text{ where } G_{bi} = 1/r_{bi} + jwC_{bi}$$
$$a_{ic} = -G_{ci} \text{ where } G_{ci} = 1/r_{ci} + jwC_{ci}$$
$$b_{ii} = y_\Sigma = y_{ee} + y_{ec} + y_{ce} + y_{cc}$$
$$b_{ic} = -y_{ec} - y_{cc}$$
$$b_{ie} = -y_{ee} - y_{ce}$$
$$c_{cc} = y_{cc}$$
$$c_{ce} = y_{ce}$$
$$c_{ci} = -y_{ce} - y_{cc}$$
$$y_{bi} = G_{bi}$$
$$y_{ci} = G_{ci}$$

where G_{bi} and G_{ci} are the base metal-intrinsic base and base-collector junction admittances per area, respectively. C_{bi} is the unit area capacitance of schottky diode at the base contact and r_{bi} is the specific base-metal contact resistance. C_{ci} and r_{bi} are the unit area capacitance and resistance of the base-collector junction, respectively. The y_{ee}, y_{ec}, y_{ce}, y_{cc} form the common base y-matrix per unit emitter area. While there are various existing models for the common-base [y], the one we used in this study is adopted from Reference [6]. They are give by:

$$y_{ee} = g_e[1 + jm(w/w_0)] + jwC_{Te}$$
$$y_{ec} = -g_{fb}[1 - j(1-m)(w/w_0)]$$
$$y_{ce} = -a_0 g_e[1 - j(1-m)(w/w_0)]$$
$$y_{cc} = g_c[1 + jm(w/w_0)] + jwC_{Tc}$$

The g_e, g_c, and g_{fb} are the emitter, collector and reverse transfer admittances, respectively. C_{Te} and C_{Tc} are the emitter and collector transition capacitances. a_0 is the dc transport factor, and m is a constant (m is assumed to be 1). w and w_0, are the operating and cut-off angular frequencies. We also adopt the assumption that g_e is much larger than g_c and g_{fb} [6]. The nonuniformity of g_e and w_0 due to the distributed nature of the junction potentials are taken into account. The ballast resistance at the emitter contact is also included.

Simplified boundary conditions are used. Fixed boundary of dc and rf base metal voltages are applied at x=0. Fixed boundary of dc and rf collector voltages are applied at $x=(L_p+L)$. Neumann boundary conditions are applied on the rest of the boundaries including those surrounding v_i network. This is regarded as the default boundary conditions in the following section. Finite difference and self-consistent ("Fix-point") numerical scheme are used to solve differential equations. With a set of initial trial solutions, v_b is solved first, then v_i and v_c are solved. One then repeats these steps using updated solutions, until the difference between two successive iterations is insignificant. From these potential distributions, emitter, base and collector currents can be calculated, and thus the microwave parameters as functions of frequency can be obtained.

RESULTS

Typical HBT structure parameters are used as the default case in the calculation. Referring to Fig. 1, the width w of the emitter mesa is 2 μm. The width of the base metal by the emitter side is 1.25 μm and the width of the gap between the emitter and the base metal is 0.2 μm. The length of the base pad L_p is 12 μm. The sheet resistances in the base metal, base layer and sub-collector layer are 0.235, 190, and 20.8 Ω, respectively. The default specific emitter and base contact resistance are 0 and 3×10^{-6} Ω-cm^2, respectively. The default capacitance of C_{bi} due to the base metal schottky contact per area is 8.76×10^{-7} F/cm^2. The transition capacitances per area at emitter and collector junctions are 3.93×10^{-7} and 1.78×10^{-8} F/cm^2, respectively.

The analysis begins with the calculation at the dc bias condition. The default dc bias point is V_{be} = 1.5 V, and V_{ce} = 3 V. The dc current gain is 50, and the ideality

factor at emitter junction is 1. The distributed nature of v_i and v_c are shown in Fig. 2. The large magnitudes of the curvature in both v_i and v_c under the emitter mesa are caused by the large vertical current transports.

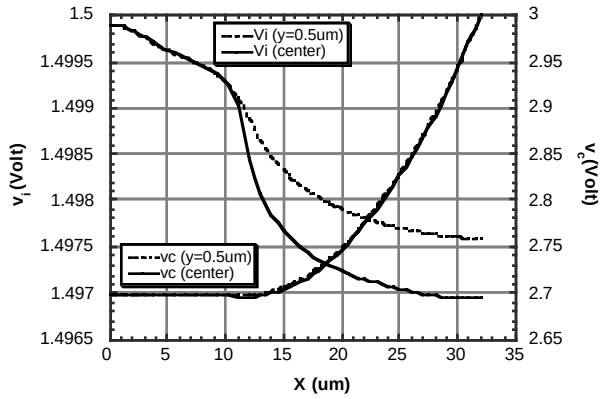

Fig. 2: The profile of the intrinsic base potential and collector potential along the side base metal (y=0.5 um), and along the center of the emitter mesa (center).

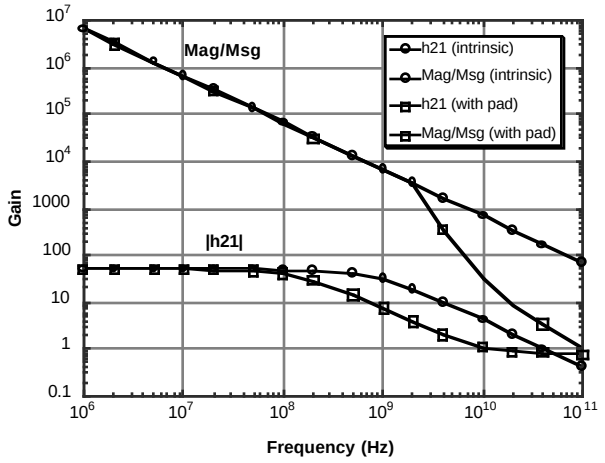

Fig. 3: The frequency dependence of the power and current gains for the intrinsic device and device with pad.

In the ac analysis, the current gain, h_{21}, and power gain, Msg or Mag, as functions of frequency are calculated. The presented power gain is the maximum available gain, Mag, if the device is unconditionally stable, or the maximum stable gain, Msg, if the device is conditionally stable. Fig. 3 shows the results for the default device. The results of the intrinsic device (i.e., HBT without pad) are also shown for comparison. The default device with base contact pad has a cut-off frequency of 10 GHz, and the unconditionally stable region exists only at frequencies larger than 20 GHz, while the intrinsic current gain has a cut-off frequency of 40 GHz, and no unconditionally stable region was found in the frequency range up to 100 GHz. The default device exhibits a level-off of h_{21} after cut-off frequency. This is due to the parasitic collector junction capacitance which conducts relatively large ac current at those frequencies.

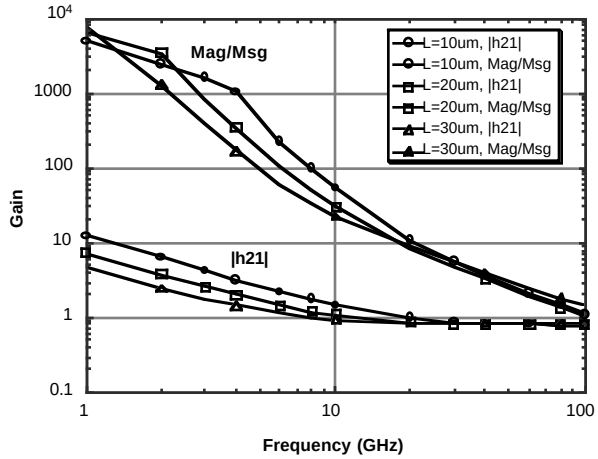

Fig. 4: The power and current gain as functions of frequency with emitter length as parameter.

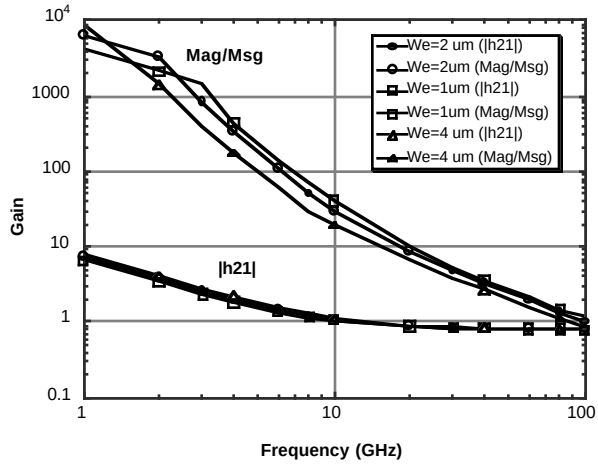

Fig. 5: The power and current gain as functions of frequency with emitter width as parameter.

The emitter length dependence is shown in Fig. 4, and the emitter width dependence is shown in Fig. 5. It is clearly shown that, although device with a larger active emitter area has a little larger maximum stable power gain, it has a smaller extracted maximum oscillation frequency. One also notes that current gain decreases as emitter length increases. This is correlated to the distributed nature of v_c which is affected by the default boundary condition implemented in this calculation. A more realistic case will be shown later. The emitter

ballast resistance dependence is also calculated. The results show that increasing emitter ballast resistance decreases both the power gain and the maximum oscillation frequency which is as expected.

It is known that high frequency performance can be improved by reducing the base-collector capacitance. This is usually achieved by using insulating ion-implantation to decrease the conductivity in both the base and collector layers in the base contact region. The modeling result for this case is shown in Fig. 6. Compared to the results shown in Fig. 4, this ion-implanted HBT has shown a larger cut-off and maximum oscillation frequencies and larger power gain.

Another device process made to improve the performance is to implement a collector contact pad closely surrounding the active area, and thus to reduce the potential nonuniformity. The boundary condition for v_c is implemented for this situation, and the results are shown in Fig. 7. One notes that the power and current gain increases, and the emitter length dependency of the current gain is indeed significantly reduced.

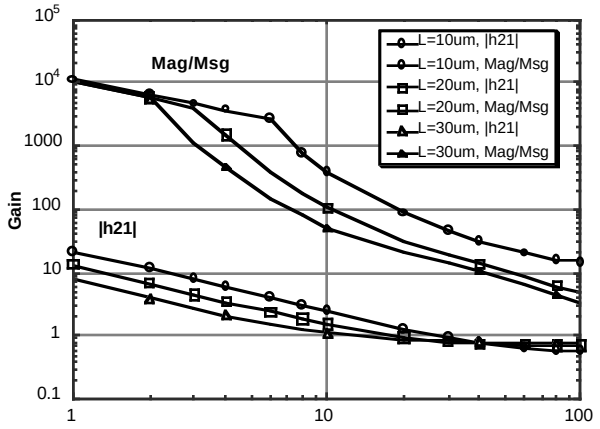

Fig. 6: The power and current gain as functions of frequency for the contact-pad-implanted devices with three different emitter lengths. The base and collector layers underneath the base contact pad are assumed insulating.

CONCLUSION

In conclusion, we have developed a TLM to study the distributed nature of HBTs. The calculation results based on the simple one-emitter-finger layout showed qualitative agreement with those expected from the traditional analytical model. This model can be further extended to develop a CAD tool to study a more complicated geometry including emitter-dot arrays in a quantitative manner. With complementing results from thermal modeling, it is hoped that the engineer may have a tool to design HBT layouts with an optimized high frequency performance.

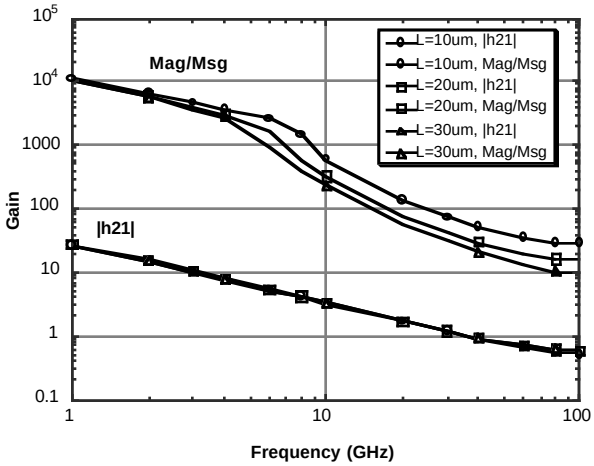

Fig. 7: The frequency dependence of the power and current gains for the same device as in Fig. 6. The collector contact encloses the active area.

REFERENCES

1. R. Dettmer, T. Jenkins, J. Barrette, C. Bozada, G. DeSalvo, J. Ebel, J. Gillespie, C. Havasy, C. Ito, K. Nakano, C. Pettiford, T. Quach, J. Sewell, and D. Via, "Effect of Device layout on the Thermal Resistance of High-Power Thermally-Shunted Heterojunction Bipolar Transistors", IEEE MTT-S Digest, pp. 1607-1610, 1996.
2. W. Liu, "Thermal Coupling in 2-Finger Heterojunction Bipolar Transistors," IEEE Trans. on Electron Devices, vol. ED-42, pp. 1033-1038, 1995.
3. E. Koenig, U. Seiler, J. Schneider, U. Erben, and H. Schumacher, "Impact of thermal Distribution and Emitter Length on the Performance of Microwave Heterojunction Bipolar Transistors," Solid-State Electronics Vol. 38, pp. 775-779, 1995.
4. L. L. Liou and B. Bayraktaroglu, "Thermal Stability Analysis of AlGaAs/GaAs Heterojunction Bipolar Transistors with Multiple Emitter Fingers," IEEE Trans. on Electron Devices, vol. ED-41, pp. 629-636, 1994.
5. W. Liu, D. Costa, and J. S. Harris Jr., "A Simplified Model for the Distributed Base Contact Impedance in Heterojunction Bipolar Transistors," Solid-State Electronics, vol. 35, pp. 547-552, 1992.
6. R. L. Prichard, "Electrical Characteristics of Transistors", McGraw-Hill, New York, 1967.